





Open Archive Toulouse Archive Ouverte (OATAO)

OATAO is an open access repository that collects the work of Toulouse researchers and makes it freely available over the web where possible

This is an author's version published in: <http://oatao.univ-toulouse.fr/24229>

Official URL: <https://doi.org/10.1016/j.bioelechem.2019.05.015>

To cite this version:

Askri, Refka and Erable, Benjamin  and Neifar, Mohamed and Etcheverry, Luc 
and Masmoudi, Ahmed Slaheddine and Cherif, Ameer and Chouchane, Habib
*Understanding the cumulative effects of salinity, temperature and inoculation size
for the design of optimal halothermotolerant bioanodes from hypersaline sediments.*
(2019) Bioelectrochemistry, 129. 179-188. ISSN 1567-5394

Any correspondence concerning this service should be sent
to the repository administrator: tech-oatao@listes-diff.inp-toulouse.fr

Understanding the cumulative effects of salinity, temperature and inoculation size for the design of optimal halothermotolerant bioanodes from hypersaline sediments

Refka Askri^a, Benjamin Erable^{b,*}, Mohamed Neifar^a, Luc Etcheverry^b, Ahmed Slaheddine Masmoudi^a, Ameer Cherif^a, Habib Chouchane^a

^a Univ. Manouba, ISBST, BVBGR-LR11ES31, Biotechpole Sidi Thabet, 2020 Ariana, Tunisia

^b Laboratoire de Génie Chimique, Université de Toulouse, CNRS, INPT, UPS, Toulouse, France

ARTICLE INFO

Keywords:

Hypersaline sediment
Halothermotolerant bioanodes
Response surface methodology
Metagenomics analysis
Statistical confrontation

ABSTRACT

The main objective of this study was to understand the interaction between salinity, temperature and inoculum size and how it could lead to the formation of efficient halothermotolerant bioanodes from the Hypersaline Sediment of Chott El Djerid (HSCE). Sixteen experiments on bioanode formation were designed using a Box-Behnken matrix and response surface methodology to understand synchronous interactions. All bioanode formations were conducted on 6 cm² carbon felt electrodes polarized at -0.1 V/SCE and fed with lactate (5 g/L) at pH 7.0. Optimum levels for salinity, temperature and inoculum size were predicted by NemrodW software as 165 g/L, 45 °C and 20%, respectively, under which conditions maximum current production of 6.98 ± 0.06 A/m² was experimentally validated. Metagenomic analysis of selected biofilms indicated a relative abundance of the two phyla *Proteobacteria* (from 85.96 to 89.47%) and *Firmicutes* (from 61.90 to 68.27%). At species level, enrichment of *Psychrobacter aquaticus*, *Halanaerobium praevalens*, *Psychrobacter alimentaris*, and *Marinobacter hydrocarbonoclasticus* on carbon-based electrodes was correlated with high current production, high salinity and high temperature. Members of the halothermophilic bacteria pool from HSCE, individually or in consortia, are candidates for designing halothermotolerant bioanodes applicable in the bioelectrochemical treatment of industrial wastewater at high salinity and temperature.

1. Introduction

The integration of microbial catalysis with electrochemistry has given rise to several innovative processes, broadly known as bioelectrochemical systems (BES), with potential energy, environmental and industrial applications such as electricity generation, hydrogen production, wastewater treatment, pollutant removal and biomolecule synthesis [1,2,3,4,5]. In BES, the efficiency of bioanodes, in terms of electron exchange kinetics, ability to recover electrons from soluble molecules and, finally, robustness, is the key to considering their industrial exploitation [2,6]. The apparent rates of electron transfer of bioanodes have greatly improved and, today, it has become possible to obtain very high current densities (greater than several tens of A/m²) by using anodes of different materials, with different geometrical designs, and with chemical, thermal or electrochemical surface treatments or coatings [6,7,8]. Along these lines, Chen et al. obtained a current density of up to 390 A/m² at 0.39 V/SHE by using multilayer structure bioanodes

for the oxidation of acetate [9]. Additionally, a power density of 1090 ± 72 mW m⁻² was achieved by using nanostructured macroporous bioanodes fabricated with natural loofah sponge as a precursor material [10]. Ketep et al. obtained >100 A/m² at 0.0 V/SCE using stainless steel foam bioanodes [11]. This evolution gives confidence in the technological feasibility of applying BES in the real industrial world or in environmental applications.

However, the majority of BES research work has been conducted in electrolyte conditions of medium temperature and low salinity, suitable for the growth of the majority of mesophilic environmental bacteria. Such factors as temperature and salinity greatly influence the energy efficiency of BES. Temperature is a critical environmental factor that plays a crucial role in increasing (i) the solubility, distribution and bioavailability of organic matter, (ii) the kinetics of biochemical and electrochemical reactions, and (iii) the mobility of ions in solutions, leading to a higher oxidation rate and, consequently, electron donation by exoelectrogenic bacteria [12,13]. For example, Liu et al. reported that a temperature rise significantly enhanced both the oxygen reduction rate on the cathode and anolyte conductivity in a microbial fuel cell [14]. Also, in the work of Adelaja et al. the maximum power density at

* Corresponding author.

E-mail address: benjamin.erable@ensiacet.fr (B. Erable).

40 °C was double that at 30 °C [15]. High salinity reduces the ohmic drop in BES by increasing electrolyte conductivity and consequently facilitating the transfer of electric charges in solution [5,16]. Unfortunately, the microbial communities that have produced the highest currents so far in BES do not operate at high salinities or high temperatures.

It is therefore accepted that the successful application of BES to the treatment of highly saline and/or hot wastewater is based on the identification and characterization of exoelectrogenic bacteria that are both tenacious and resilient under these particularly extreme conditions. Halothermophilic microorganisms are thus suitable candidates for the treatment of the high saline wastewaters generated, for example, in the seafood processing (8 to 20 g/L), textile dyeing (2 to 10 g/L), petroleum (few g/L to 300 g/L), and tannery industries (40 to 80 g/L) [17,18]. Some halophilic and/or thermophilic bacterial species isolated from extreme natural or industrial environments have been reported to display electroactive properties [19,20]. In particular, sediments from salt marsh [7,8], saline microbial mats and salt lakes [21], saline ponds [22], the Red Sea [17], the Great Salt Lake [2], and Sambhar Lake [6] have been investigated to select electroactive bacterial biofilms. In the majority of these studies, a positive correlation between salinity and current generation has been demonstrated. However, all these studies were carried out at temperatures lower than or equal to 37 °C and so none of this work examined the combined effect of increased salinity and high temperature on the bioanode current production, yet the salinity and thermal tolerance of halothermophilic microorganisms would make it possible to consider the design of halothermotolerant bioanodes that would be truly suitable for the treatment of hot, highly saline wastewater. In addition, the approaches used to improve the performance of bioanodes under saline or thermal conditions have so far been carried out by monitoring the influence of a single factor at a time, by following a single experimental response, which is often only the generation of current [3,6,7,8,15,21,22]. These approaches, known as one-variable-at-a-time optimization, do not include the interactive effects between the variables studied. Consequently, this optimization does not depict the effects of all the factors on the response. To overcome this limitation, multivariate statistical techniques, such as response surface methodology (RSM), based on fitting a polynomial equation to the experimental data with the objective of making statistical previsions, could be applied as appropriate tools. RSM can be appropriately applied when a response or a set of responses of interest is influenced by several variables [23,24]. It can be concluded from the published literature that current practices in the area of process improvement recommend employing RSM to express the output parameters (responses), in terms of input factors.

The main objective is to simultaneously optimize the levels of these variables so as to attain the best system performance. Such tools are actually applied mainly in the optimization of analytical chemistry processes such as chromatographic methods, sorption processes, and biomolecule production by microorganisms [25,26,27,28,29]. These statistical designs are now attracting the attention of researchers for (microbial) process optimization. As described by Bezerra et al. [23], application of RSM is a multi-step optimization technique successively organized into (i) the selection of independent variables having major effects on the system, (ii) the choice of the experimental design and the execution of the experiments, (iii) the mathematical-statistical treatment of the experimental data obtained, by fitting a polynomial function, (iv) the evaluation of the model's fitness, and (v) obtaining the optimum values for each variable studied. Despite their increasing popularity, these tools have not been widely used for the optimization of BES efficiency.

In southern Tunisia, there is a large terrestrial lake, Chott El-Djerid, which is covered by an extensive salt pan during the dry season [18]. Its evaporitic environment is characterized by extreme conditions including, dryness, elevated UV irradiation and relevant salt concentration of chlorides and sulfates varying between 200 and 330 g/L [30]. Desert climatic conditions also prevail at Chott El Djerid, with an average

temperature ranging from 40 to 55 °C. Extremophiles inhabiting this particular ecological niche have had to evolve systems to deal with the harsh conditions: mainly high salinity and elevated temperature. Consequently, sediment from this extreme environment is a promising potential source of exoelectrogenic halothermotolerant microorganisms for enriching the microbial communities on electrodes. The aim of this study was thus to demonstrate, for the first time, that a halothermotolerant electrocatalytic bioanode could be designed from Hypersaline Sediment of Chott El Djerid (HSCE) under combined high temperature and hypersaline conditions. Although exoelectrogenic biofilms have been enriched on anodes operated under either hypersaline [6,8] or high temperature [19,20] conditions, there have been no studies showing current generation under both these conditions. Once the electroactivity of HSCE inoculum had been proved, the cumulative effects of temperature (40 to 50 °C), salinity (100 to 200 g/L NaCl), and sediment inoculation size (10 to 30%) were crossed using response surface methodology (RSM) to investigate the effect of interaction among these variables on the formation of bioanodes. Additionally, the maximum current production, the biofilm microscopic structure on the electrode and the anodic bacterial communities were systematically confronted during or at the end of bioanode formation. Both predicted and experimental results showed that HSCE could be used for designing halothermotolerant bioanodes for future BES operations under high salinity and high temperature conditions.

2. Materials and methods

2.1. Collection of hypersaline sediment samples

Hypersaline sediments used as the inoculum were sampled from a continental salt lake, Chott El Djerid, located in the south of Tunisia (N 33°59'965" E 08° 25'332") during the dry season in April (Fig. 1). Samples were a mixture of saturated water and sediment (2:1 vol.:vol.) collected from the surface, temperature was 38 °C and conductivity higher than 200 mS cm⁻¹. Samples were stored in closed plastic boxes at +4 °C until bioanode formation experiments were initiated.

2.2. Medium composition

The nutrient medium contained (g/L): 0.5 g K₂HPO₄, 1 g NH₄Cl₂, 2 g MgCl₂, 0.1 g CaCl₂. Sodium lactate (5 g/L) was added as the anodic substrate for all experiments. NaCl concentration (g/L), temperature (°C) and inoculum size (%) were adjusted to appropriate values as described in the Box-Behnken design (Table 1) before the start of bioanode formation experiments.

2.3. Construction of microbial electrolysis cells (MECs) and electrochemical protocol

All experiments were performed in glass MEC reactors with a total volume of 750 ml (150 ml head space), filled with nutrient medium and inoculated with hypersaline sediment from Chott El Djerid (HSCE). MEC reactors were deaerated for 15 min with a continuous gas flow of N₂ before the experiments start. Sixteen MEC experiments were carried out with a working electrode (WE) made of a porous carbon felt of 6 cm² projected surface area electrically connected to a platinum wire (1 mm diameter and 15 cm long) and polarized at -0.1 V/SCE, a platinum grid used as the counter electrode (CE), and a saturated calomel reference electrode (+0.24 V/SHE) located between the counter and the working electrodes. The distance between the WE and the CE was fixed at 6 cm in all experiments. A detailed scheme of the experimental set-up is shown in Fig. 2. All electrodes were connected to a VSP multichannel potentiostat (Biologic SAS) equipped with EC lab software. Constant polarization was applied on the working electrode at -0.1 V/SCE (chronoamperometry) [31,32], the average current was recorded every 20 min.

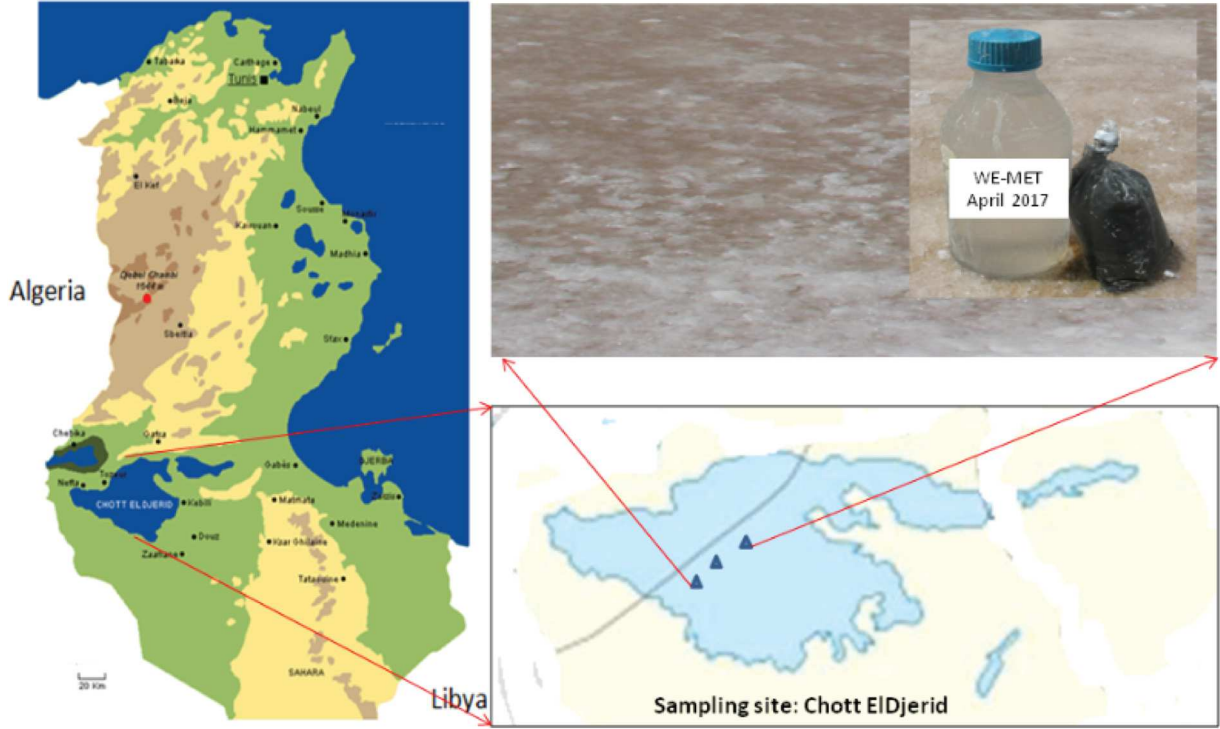


Fig. 1. Location of sampling sites: Chott El Djerid hypersaline environment in southern Tunisia.

2.4. Study of combined effects of salinity, temperature and inoculum size on current production using response surface methodology (RSM)

To investigate the impact of salinity, temperature and inoculation size on the current production response, surface methodology using a Box-Behnken Design (BBD) was applied.

The BBD is a class of rotatable (or nearly so) second-order designs based on three-level incomplete factorial design. The number of experiments (N) required for the development of BBD is defined as $N = 2k(k-1) + C_0$, where k is the number of factors and C_0 is the number of central points [33].

The BBD design involved three process variables: inoculum size (η_1), temperature (η_2) and NaCl concentration (η_3), each at three equidistant levels (-1, 0, +1), with four replicates at the center point. We thus obtained a total of 16 experiments (Table 2). The graphical representation of the three-variable BBD (Fig. 3) can be seen as a cube where experimental points are located in the middle of the cube edges (12 experiments) and at the center of the cube (4 experiments). Parameters corresponding to the central point (0,0,0) are repeated four times to establish that the experimental data is within the normal dispersion and that repeatability is ensured, and also to estimate the pure error variance. Selected boundaries of the variables for the BBD (Table 1) were based on preliminary experimental tests performed on HCSE as well as results of previous studies [3,19,20].

When evaluating the relationship between the response (current production) and the process variables (η_1 , η_2 , and η_3), interaction between any two process variables can be described. Commonly, a second-order model is utilized to find a suitable approximation for the

functional relationship between η_1 , η_2 , and η_3 and the response surface Φ (A/m^2) (Eq. (1)):

$$\Phi = \delta_0 + \sum_{i=1}^k \delta_i \eta_i + \sum_{i=1}^k \delta_{ii} \eta_{ii}^2 + \sum_i \sum_j \delta_{ij} \eta_i \eta_j + \varepsilon \quad (1)$$

ε is the random error.

In matrix form, the above equation can be written as:

Φ (A/m^2) = $\delta \eta + \varepsilon$ and the solution can be obtained using the matrix approach,
 $\delta = (\eta^T \eta)^{-1} \eta \Phi$.

To apply the BBD approach, the NemrodW software was used [34]. After acquiring data related to each experimental point, we fitted a mathematical equation describing the behavior of the response according to the levels of the values studied. A regression model containing 10 coefficients, including the linear and quadratic effect on variables and

Table 1
Experimental domain of the Box-Behnken design.

	Unit	Center	Step of variation
Inoculum size (η_1)	%	20	10
Temperature (η_2)	°C	45	5
NaCl (η_3)	g/L	150	50

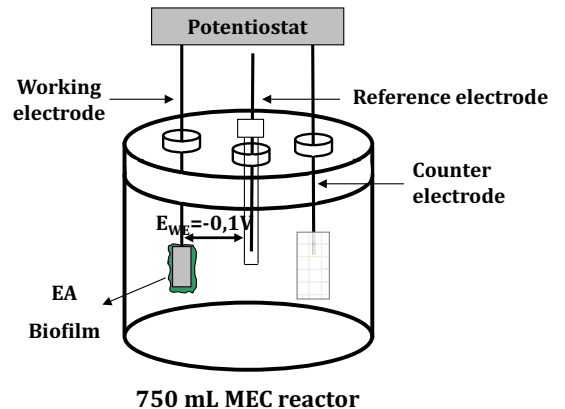


Fig. 2. Schematic representation of a MEC reactor equipped with a 3-electrode system.

Table 2
Statistical design in coded and natural variables and the corresponding experimental and predicted current production.

Reactors	η_1	η_2	η_3	Inoculum size (%)	Temperature (°C)	Salinity (g/L)	Current production (A/m ²)	
							Experimental	Predicted
R ₁	-1	-1	0	10.00	40.00	150.00	3.70	4.538
R ₂	1	-1	0	30.00	40.00	150.00	4.00	3.813
R ₃	-1	1	0	10.00	50.00	150.00	3.80	3.988
R ₄	1	1	0	30.00	50.00	150.00	4.60	3.763
R ₅	-1	0	-1	10.00	45.00	100.00	4.00	3.950
R ₆	1	0	-1	30.00	45.00	100.00	4.50	5.475
R ₇	-1	0	1	10.00	45.00	200.00	7.50	6.525
R ₈	1	0	1	30.00	45.00	200.00	4.00	4.050
R ₉	0	-1	-1	20.00	40.00	100.00	6.20	5.413
R ₁₀	0	1	-1	20.00	50.00	100.00	3.60	3.463
R ₁₁	0	-1	1	20.00	40.00	200.00	4.20	4.338
R ₁₂	0	1	1	20.00	50.00	200.00	4.90	5.688
R ₁₃	0	0	0	20.00	45.00	150.00	6.70	6.700
R ₁₄	0	0	0	20.00	45.00	150.00	6.70	6.700
R ₁₅	0	0	0	20.00	45.00	150.00	6.60	6.700
R ₁₆	0	0	0	20.00	45.00	150.00	6.80	6.700
R17 Optimal conditions				20	45	165	6.98	6.74

the linear effect on interactions was generated by the software (Eq. (2)):

$$\Phi \text{ (A/m}^2\text{)} = \delta_0 + \delta_1 \eta_1 + \delta_2 \eta_2 + \delta_3 \eta_3 + \delta_{11} \eta_1^2 + \delta_{22} \eta_2^2 + \delta_{33} \eta_3^2 + \delta_{12} \eta_1 \eta_2 + \delta_{13} \eta_1 \eta_3 + \delta_{23} \eta_2 \eta_3 \quad (2)$$

where δ_0 is the model constant; η_1 , η_2 and η_3 are the independent variables; δ_1 , δ_2 and δ_3 are the linear coefficients; δ_{12} , δ_{13} and δ_{23} are the cross-product coefficients, and δ_{11} , δ_{22} and δ_{33} are the quadratic coefficients.

A polynomial regression analysis was used to determine the values of the coefficients and the quality of the model was tested by the coefficient of determination R^2 and two-way ANOVA. The main focus of the two-way ANOVA was to compare the variation due to the change in the combination of variable levels with the variation due to random errors inherent in the measurements of the response generated [28,35]. ANOVA employs sum of squares and F statistics to find the relative importance of the processing variables analyzed, the measurement errors, and uncontrolled parameters. It was used to check the adequacy of the model for the responses in the experiments.

Besides ANOVA verification of the adequacy of the statistical model, additional verification experiments were carried out under the optimal conditions predicted by the model.

2.5. Epifluorescence microscopy

At the end of each bioanode formation experiment, working electrodes covered by HSCE enriched biofilms were immediately stained

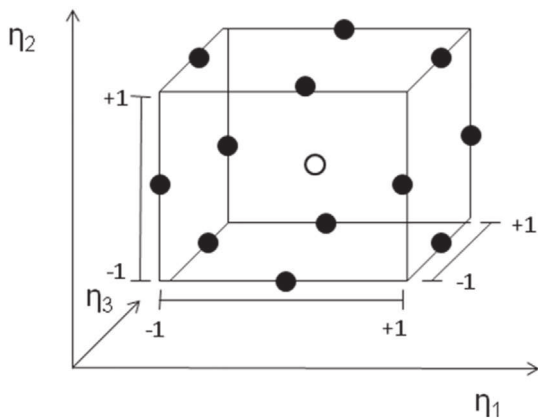


Fig. 3. Schematic cube graphical representation of the three-variable Box Behnken Design.

with acridine orange 0.01% (A6014 Sigma) and incubated for 10 min. Acridine orange stains both the intracellular and extracellular nucleic acids and thus gives a fair representation of the global biofilm structure. Then bioanode coupons were washed carefully with sterile physiological water and dried at ambient temperature overnight. Biofilms were then imaged with a Carl Zeiss Axio Imager-M2 microscope (Carl Zeiss, Oberkochen, Germany) equipped for epifluorescence with an HXP 200C light source and the Zeiss 09 filter (excitor HP450r HP450200 C light source). Images were acquired with a digital camera (Zeiss AxioCam MRm) every 0.5 mm along the Z-axis and the set of images was processed with the Zen (Carl Zeiss) ® software.

2.6. Bacterial anode analysis

Biofilms were sampled from carbon felt electrodes in order to phylogenetically characterize bacteria occurring on the bioanode. Genomic DNA extraction was performed using a *NucleoSpin® Soil kit* according to the manufacturer's instructions. Yield and quality of DNA and PCR products were checked by agarose gel electrophoresis and Nanodrop. To analyze the composition of the bacterial communities in the different biofilms, Illumina Miseq 16S rRNA sequencing was performed. The 16S rRNA gene V4 variable region PCR primers 515/806 were used in single-step 30 cycles PCR using the HotStarTaqPlus Master Mix Kit (Qiagen, USA). Sequencing was performed at MR DNA (www.mrdnlab.com, Shallowater, TX, USA) on an Ion Torrent PGM following the manufacturer's guidelines. Sequences were depleted of barcodes and primers, then sequences <150 bp or with ambiguous base calls or with homopolymer runs exceeding 6 bp were all removed. OTUs were then generated and clustered at 97% similarity. OTUs were taxonomically classified using BLASTn against two databases RDPII (<http://rdp.cme.msu.edu>) and NCBI (www.ncbi.nlm.nih.gov).

3. Results and discussion

3.1. Analysis of synchronous effects of salinity, temperature and inoculum size on design of halothermotolerant bioanodes

Response surface methodology was applied to investigate the combined effects of salinity, temperature and HSCE inoculum size on HSCE-based bioanode current production. A three variable BBD was used to explore interactions among the selected variables. Details of the 16 experimental runs with the set of input parameters used are given in Table 2.

NemrodW software was used to design and randomize the experiments [34]. Randomization guaranteed that the conditions of an

experiment were independent of the conditions of previous experiments and did not predict the conditions of subsequent ones. Randomization was crucial for drawing correct, defensible conclusions from the experiment.

Stable maximal current densities, recorded at least for a 12 h time period, ranging from 3.6 to 7.5 A/m² were obtained after using the set of 16 experiments of the BBD. As shown in Table 2, the low levels of salinity (R5, R6 and R10), temperature (R1, R2 and R11) and inoculum size (R1, R3, and R5) resulted in low current production, between 3.6 and 4.2 A/m². Similarly, high levels of salinity (R8, R11 and R12), temperature (R3, R4, R10, R12) and inoculum size (R2, R4, R6, R8) generated low current, ranging from 3.6 to 4.9 A/m². However, medium levels of salinity, temperature and inoculum size (R13, R14, R15 and R16) provided higher current density, between 6.6 and 6.8 A/m². Interestingly, high values of current production were obtained under conditions different from those described above. In reactor R7, a current density of 7.5 A/m² was obtained at a high level of salinity (200 g/L), medium level of temperature (45 °C) and low size of inoculum (10%). Then, in reactor R9, current density of 6.20 A/m² was obtained at a low level of salinity (100 g/L), low level of temperature (40 °C) and medium level of inoculum (20%). These findings show that understanding the interactions between these variables is of great interest. To analyze the accuracy of the data and the interactions between variables, the significance of the results at a selected confidence level were considered via a multiple-regression fit model and ANOVA.

ANOVA is an important statistical tool widely used to further verify the accuracy of models. The results of the model are summarized in Table 3, including the sum of squares (SS), mean square (MS), Fisher's F-test values (F values) and P-values, the lack of fit of the model and R² (see supplementary data explaining how these parameters were determined). The P-value is used to check whether the F value result is statistically significant or not [28,36,37]. R² should be examined throughout the analysis because this parameter indicates the percentage of variance explained by the model [36]. R² indicates the accuracy and goodness of fit of the model and, if the data or model is satisfactory, then the R² should be close to 1.0.

Data from Table 3 showed that the R² value was 0.934, indicating a high degree of correlation between the observed and predicted values for current production. From the R² value, it was concluded that only 6.6% of the variation for current production could not be explained by the model.

As shown in Table 3, the F value was 32.3343, indicating that the model was significant and the majority of variation in the responses could be explained by the regression equation. Furthermore, the P-value <.0001 indicated that the model terms were statistically significant.

According to the coefficients shown in Table 4, the quadratic term coefficients (δ_{11} , δ_{22} and δ_{33}), and the interaction terms (δ_{13} and δ_{23}) had highly significant effects on current production ($P < 0.0001$), followed by the linear term coefficients δ_1 and δ_3 , with significant effect ($P < .01$), and then the linear term coefficient δ_2 with a significant effect ($P < .01$). However, the interaction term δ_{12} was not significant ($P > .05$). It was concluded that, in the model, the factor having most influence on current production was the interaction between salinity and temperature, followed by salinity and temperature as single effects.

Table 3
ANOVA of the response surface for the quadratic model.

Source of variation	Sum of squares	DF	Mean of squares	F values	P values	Significance	R ²
Model	19.5400	9	1.6156	32.3343	<0.0001	***	0.934
Residual	0.4677	6	0.7796				
Lack of fit	0.4657	3	0.1552	3.8750	0.1692	NS	
Pure error	0.0200	3	0.0675				
Total	22.2175	15					

*** Significant at the level 99.9%. N.S. non-significant.

Table 4
P values of studied variables and their quadratic and interaction terms.

Name	Coefficient	F, Inflation	Stand Dev.	t.exp.	P values
δ_0	6.700		0.041	164.12	<0.0001***
δ_1	-0.237	1.00	0.029	-8.23	<0.01**
δ_2	-0.150	1.00	0.029	-5.20	<0.05*
δ_3	0.287	1.00	0.029	9.96	<0.01**
δ_{11}	-1.200	1.00	0.041	-29.39	<0.0001***
δ_{22}	-1.475	1.00	0.041	-36.13	<0.0001***
δ_{33}	-0.500	1.00	0.041	-12.25	<0.0001***
δ_{12}	0.125	1.00	0.041	3.06	=0.54 NS
δ_{13}	-1.000	1.00	0.041	-24.49	<0.0001***
δ_{23}	0.825	1.00	0.041	20.21	<0.0001***

NS: non significant.

*** Significant at the level of 99.9%.

** Significant at the level 99.0%.

* Significant at the level 95.0%.

However, the interaction between inoculum size and temperature was relatively weak ($P = .54$).

The highly significant effects on current production of the interaction terms δ_{23} and δ_{13} demonstrated the combined effects of salinity, temperature and HSCE inoculum size on HSCE-based bioanode current production.

Using values of coefficients from Table 4, the final polynomial quadratic equation for current production was determined as follows (Eq. (3)):

$$\Phi = \text{current production (A/m}^2\text{)} = 6.7 - 0.237 \eta_1 - 0.15 \eta_2 + 0.287 \eta_3 - 1.2 \eta_{11} - 1.475 \eta_{22} - 0.5 \eta_{33} + 0.125 \eta_1 \eta_2 - 1 \eta_1 \eta_3 + 0.825 \eta_2 \eta_3 \quad (3)$$

The values of the coefficients in the model are related to the effect of these variables on the current production. Given that η_1 , η_2 and η_3 are the coded values for inoculum size, temperature and salinity, respectively. The previous equation could be expressed in the following form (Eq. (4)):

$$\text{Current density (A/m}^2\text{)} = 6.7 - 0.237 [\text{inoculum size}] - 0.15 [\text{temperature}] + 0.287 [\text{salinity}] - 1.2 [\text{inoculum size}]^2 - 1.475 [\text{temperature}]^2 - 0.5 [\text{salinity}]^2 + 0.125 [\text{inoculum size}] \times [\text{temperature}] - 1 [\text{inoculum size}] [\text{salinity}] + 0.825 [\text{temperature}] [\text{salinity}] \quad (4)$$

Previous statistical analyses justify the use of the quadratic model in this study as a tool for prediction.

3.2. Model prediction of the effect of inoculum size, temperature, and salinity on current production

The interaction effects of salinity, temperature, and inoculation size on bioanode current density production were examined by plotting the response area curves against two significant independent variables, keeping the other variable at constant level. Response surface plots and their corresponding contour plots for predicted current density are shown in Fig. 4. These plots are suitable tools to understand how the interaction between the variables studied affects current production. A circular contour line indicates that the interaction between two compared independent variables is weak, while an oval or elliptical contour line indicates a significant interaction between the two independent variables [28,38].

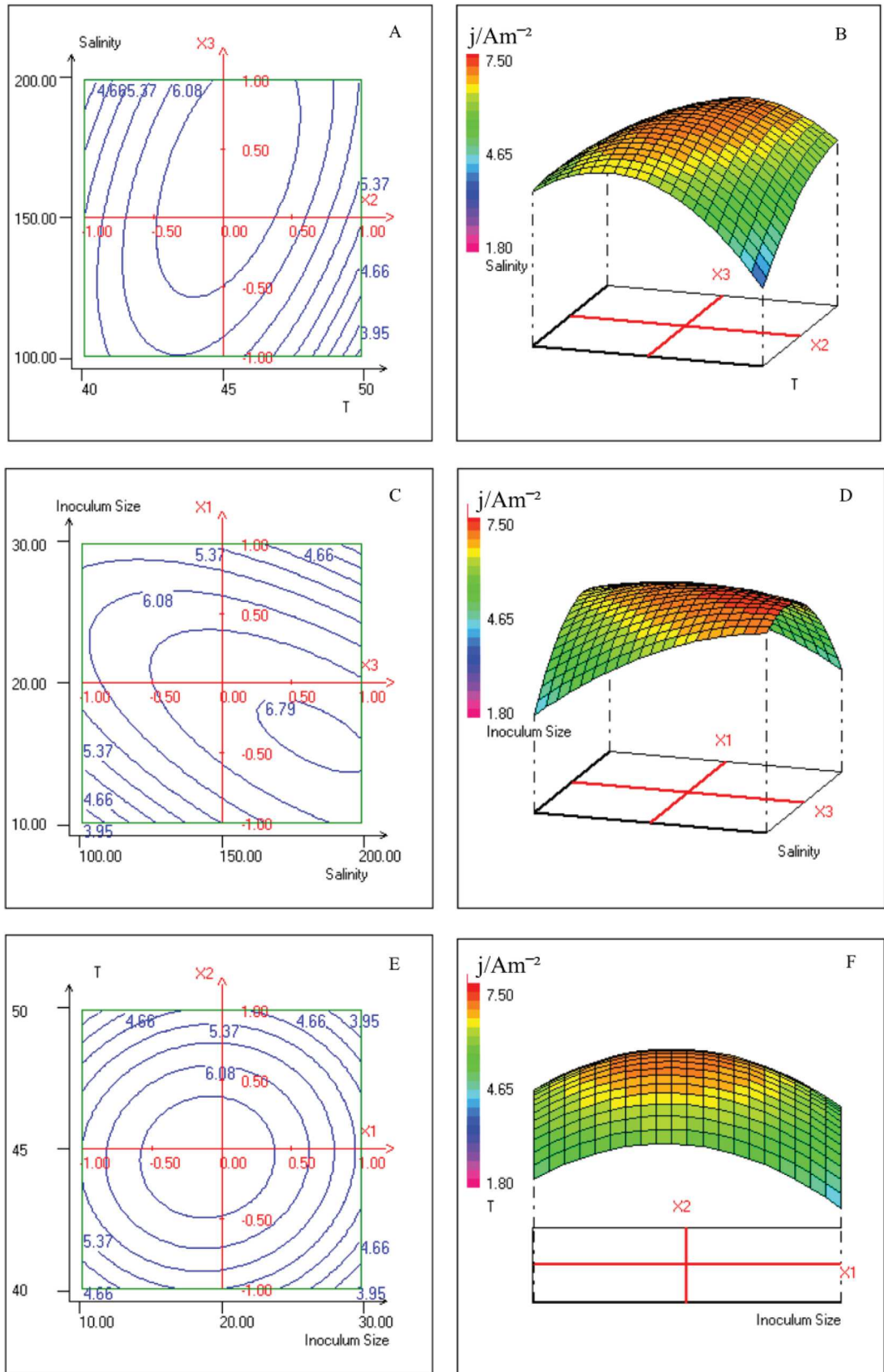


Fig. 4. The 2D-contour plots and 3D-response surface of current production j/Am^{-2} versus the tested variables: salinity and temperature (T) [A and B]; inoculum size and salinity [C and D]; temperature (T) and inoculum size [E and F].

Figs. 4.A and 4.B describe the two-dimensional (2D) counter plot and corresponding three-dimensional (3D) response surface plot expressing the crossed effect of salinity (η_3) and temperature (η_2) on the

maximum current density when the inoculation size (η_3) was kept constant at the center level (20%). At 40 °C, the current density remained constant (5.4 A/m²) in a salinity range of 100 to 150 g/L, then decreased

slightly (5.0 A/m) for salinity values above 150 g/L. However, at 45 °C, the current density rose from 5.4 to 5.9 A/m² for a salinity of 100 g/L, then increased significantly (6.7 A/m²) when the salinity increased from 100 to 175 g/L. Above this limit value of salinity, the current density started to decline. Similarly Figs. 4.C and 4.D show that current density increased when salinity rose from 100 to 175 g/L at a constant temperature fixed at 45 °C. Further increase in salinity beyond 175 g/L induced a gradual fall in current density. The information provided by the Figs. 4.C and 4.D reveal that salinity (from 100 to 175 g/l) and temperature (from 40 to 47 °C) impacted the current production positively. However, salinity >175 g/l and temperature beyond 47 °C lowered the production of current by bioanodes slightly.

By partial differentiation of the established second-order regression model, the optimum conditions for maximum current production were established as: 20% inoculum size, 45.5 °C temperature, and 164 g/L salinity. Under these conditions, the second-order model predicted a maximum current production of 6.74 ± 0.04 A/m².

3.3. Experimental validation of the model

In addition to the verification through ANOVA, the adequacy of the statistical model was validated through three additional verification experiments carried out under the theoretically optimal conditions predicted by the model and leading to the highest current production.

As can be seen in Fig. 5, the variability in current density was low. Actually, from one triplicate experiment to another, the current-time curves exhibited a similar general trend and the absolute current densities were not different. The three replicates showed a maximum current density around 6.98 A/m² with a standard deviation of <1%. It is worth noting that these findings are of crucial importance because, in less controlled experimental systems like MFCs without potentiostatic control, the results are hardly ever so reproducible [39,40].

The concordance between the experimental results and the results predicted by the statistical model is rather strong (<4% of difference). The experimental mean current density production was 6.98 ± 0.06 A/m², agreeing well with the predicted value of 6.74 ± 0.04 A/m², and indicating the validity and the robustness of the model.

Additionally, the average current density (6.98 ± 0.06 A/m²) measured for the optimized HSCE based bioanodes was within the range of findings reported by previous studies using other saline or thermophilic environments [20,41]. Miceli et al. obtained current densities of 1.5–10.8 A/m² from various anaerobic environmental samples including saltwater samples enriched with progressively increasing salt concentrations (20 g/L NaCl and 3 g/L MgCl₂) [41]. Current densities of 5.0–8.3 A/m² were generated by acetate-fed pure culture of alkaliphilic *Geoalkalibacter ferrihydriticus* under slightly saline conditions (10 g/L) in dual-chamber MECs using anodes polarized at +0.07 V/SHE [20].

However, the elevation of salinity to 17 g/L caused a decrease in current production of >50% (2.4–3.3 A/m²). Using saline sediment from the Red Sea as the inoculum for enriching the exoelectrogenic community on anodes of an MEC, Shehab et al. reported current density of about 6.8 ± 2.1 A/m² with bioanodes operated at a potential of +0.2 V/Ag/AgCl (+0.405 V/SHE), fed with acetate under high temperature (70 °C) and hypersaline (250 g/L) conditions [42].

3.4. Biofilm morphology

At the end of bioanode formation at –0.1 V/SCE, biofilms colonizing working electrodes extracted from reactors R₃, R₇ and R₁₇ were imaged by epifluorescence microscopy (Fig. 6). These biofilms were obtained at different salinities (150, 200, 165 g/L), temperatures (50, 45, 45 °C) and inoculation ratios (10, 10, 20%) and produced different current densities: 3.80, 7.50 and 6.98 A/m², respectively (Table 2).

Increasing NaCl concentration from 150 to 165 and then to 200 g/L impacted the distribution of microorganisms at the carbon fiber scale in felt electrodes. As shown in Fig. 6 A, B and C, two different kinds of biofilm structure were observed depending strongly on the salinity. For NaCl concentrations of 150 and 165 g/L, biofilms covered the interstitial spaces between carbon fibers (Fig. 6 A and B). Increasing the NaCl concentration to 200 g/L increased the thickness of the biofilm layer on the fibers (Fig. 6 C) but areas between fibers remained empty and dark. In the field of electroactive halotolerant anodic biofilms, Rousseau et al. report similar observations regarding the structure of biofilms formed in salty electrolytes with concentrations between 30 and 60 g/L of NaCl [8]. They concluded that, at the highest salinity (60 g/L NaCl), the bioanode performance was affected by the modification of the biofilm structure and a decrease in the percentage of bacterial coverage on the felt fibers. Interestingly, in our study, conducted in a higher range of NaCl concentrations, despite changes in the biofilm architecture around the carbon fibers, the performance of the bioanode was not affected. Rousseau et al. [8] indicated that the reduction in current density seen at the highest salinity (60 g/L) was due to the restricted structure of the biofilm, which was rarefied in the interstitial spaces but formed sheaths around the fibers. These results do not agree with our findings, where, although rarefied, the biofilm in the interstitial spaces remained efficient. This difference was probably dependent on the nature of the microbial community colonizing the anode.

3.5. Bacterial analysis of the anodic biofilm

Based on the quality of DNA extracted, the salinity, the temperature and the current density produced, four biofilms, named B1, B3, B7 and B17 from reactors R1, R3, R7 and R17, respectively, were selected for bacterial analysis. A glance at the bacterial population of these biofilms

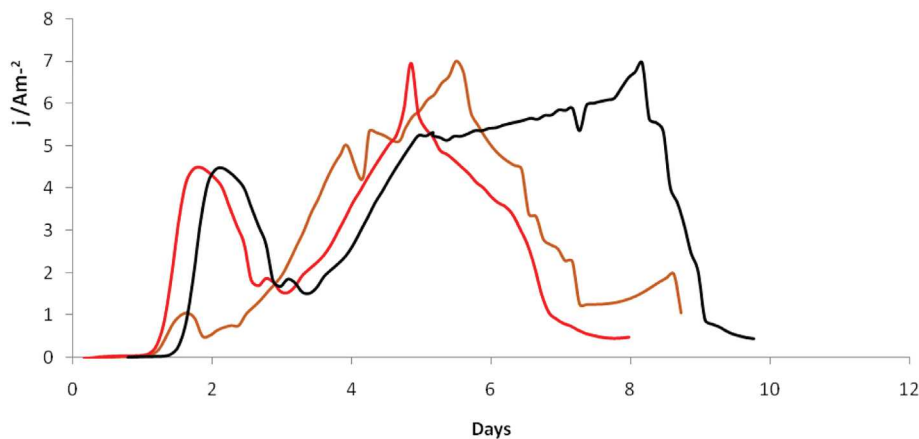


Fig. 5. Evolution of the current density (j/Am^{-2}) versus time (days) for triplicate experiments on a carbon felt electrode of 6 cm² projected surface area polarized at –0.1 V/SCE in a liquid medium under optimal conditions determined by the statistical model: salinity 165 g/L, temperature 45 °C and inoculum size of 20%. (— triplicate 1, — triplicate 2, — triplicate 3).

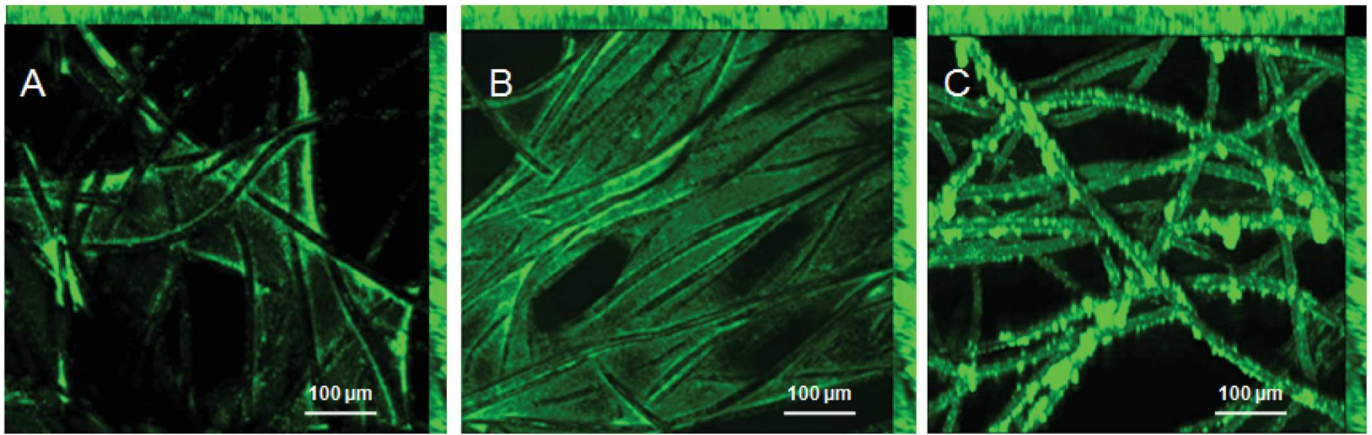


Fig. 6. Bioanode imaging by epifluorescence microscopy after staining electrode surface with acridine orange to localize microbes in the exopolymeric matrix. Bioanodes were formed at NaCl concentrations of 150 (A), 165 (B) and 200 g/L (C).

(Fig. 7) indicates a very high abundance of two phyla: *Proteobacteria* (from 85.96 to 89.47%) and *Firmicutes* (from 61.90 to 68.27%). *Proteobacteria* were enriched in biofilms from reactors 1 and 7, at close relative abundances of 89.47 and 85.96%, respectively. However, they showed different current productions, of 3.4 and 7.5 A/m², respectively. *Firmicutes* were enriched in biofilms from reactors 3 and 17, with relative abundances of 68.27 and 61.90%, respectively. B3 and B17 produced current densities of 4 and 6.98 A/m², respectively. The other part of the community was made up of various phyla (*Bacteroidetes*, *Synergistetes*, *Chloflexi*, and *Actinobacteria*) the percentage of each always being <2%. It is interesting to point out that the *Thermotogae* phylum colonized biofilm B17 at a relative abundance of 10.89%. Very few studies have described this phylum as electrogenic. At the species level (Fig. 8), (from the detected phyla, *Proteobacteria*, *Firmicutes* and *Thermotogae*), the most prevalent bacteria in B1 and B7 were *Halomonas* spp and *Psychrobacter aquaticus* with relative abundances of 82.91% and 65.02%, respectively. B3 shows a bacterial profile with the enrichment of *Bacillus* sp (24.4%), *Halanaerobium praevalens* (20.3%), *Holomonas* spp (13.73), *Marinobacter hydrocarbonoclasticus* (11.12%) and *Halomonas*

sp (5.3%). However, in the case of B17, the microbiome was dominated by *Psychrobacter aquaticus* (43.03%), *Psychrobacter alimentarius* (5.82%), *Halanaerobium praevalens* (22.1%), *Psychrobacter alimentarius* (5.82%) and *Marinobacter hydrocarbonoclasticus* (5.51%).

In the context of isolation of halotolerant bacterial in controlled enrichment conditions (acetate as electron donor, -0.3 V / Ag/AgCl as electrode, 20 g/L NaCl and 3 g/L MgCl₂) Miceli et al. obtained a current density of 4.23 A/m² of biofilm population enriched in single-chamber microbial electrolysis cells [41]. Polarizing the electrode at -0.2 V / Ag/AgCl in the presence of 17 g/L NaCl decreased the current density produced by *Geoalkalibacter subterraneus* to 3.3 A/m² [41]. However, the highest current density, of 4.68 ± 0.54 A/m², was obtained when a graphite planar electrode was polarized at +0.2 V / SCE, under 35 g/L of NaCl [43]. The strains *Geoalkalibacter subterraneus* and *Desulfuromonas acetoxidans* were found in abundance in biofilms colonizing anode electrodes when saline and hypersaline inocula were used and, specifically, when acetate and butyrate were added as substrate. In this study, MECs fed with lactate demonstrated that

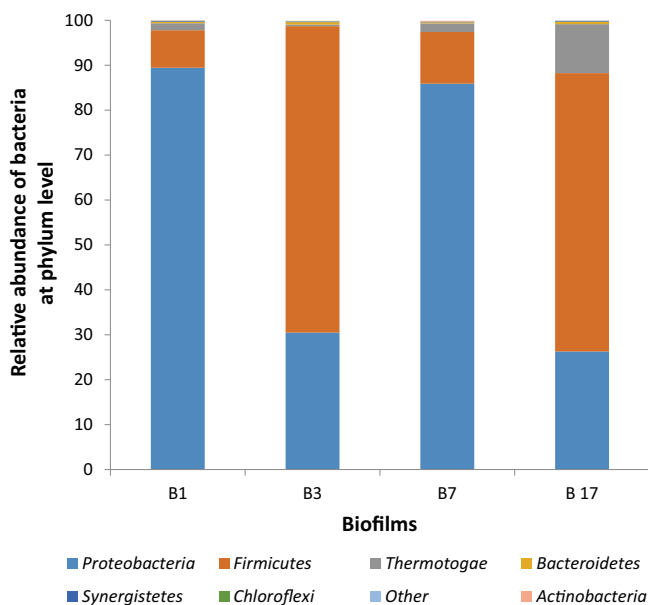


Fig. 7. Bacterial distribution of biofilm communities at phylum level. B1 (salinity 150 g/L, temperature 40 °C and inoculum size of 10%), B3 (salinity 150 g/L, temperature 50 °C and inoculum size of 30%), B7 (salinity 200 g/L, temperature 45 °C and inoculum size of 10%), and B17 (salinity 165 g/L, temperature 45 °C and inoculum size of 20%).

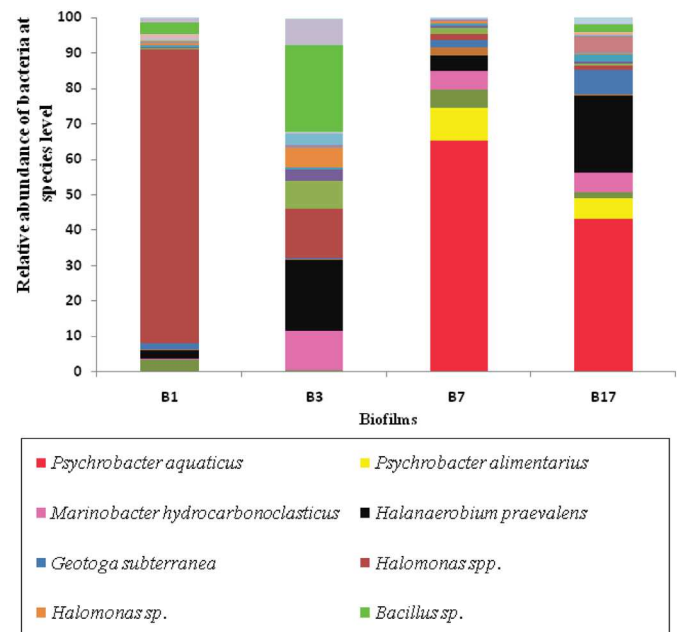


Fig. 8. Bacterial distribution of biofilm communities at species level. B1 (salinity 150 g/L, temperature 40 °C and inoculum size of 10%), B3 (salinity 150 g/L, temperature 50 °C and inoculum size of 30%), B7 (salinity 200 g/L, temperature 45 °C and inoculum size of 10%), and B17 (salinity 165 g/L, temperature 45 °C and inoculum size of 20%).

Psychrobacter aquaticus, belonging to the dominant family *Moraxellaceae*, was the most prevalent bacteria in biofilms and was correlated with the highest current density. The presence of *Psychrobacter aquaticus* and *Psychrobacter alimantarius* under such experimental conditions was somewhat surprising since it is more frequently found in cold and other non-polar environments of low water activity [44]. However, no previous studies have described the presence of these strains either in anodic biofilm or in Chott el Djerid samples. This is a promising result that encourages research aiming to isolate and characterize *Psychrobacter* strains and test their bioelectrochemical behavior in pure culture. According to Lasa et al., *Psychrobacter* strains have shown valuable activities involved in bioremediation by producing carbonic anhydrase enzymes [44]. This feature makes the use of this strain possible in coupled bioelectricity generation and saline wastewater treatment. *Marinobacter hydrocarbonoclasticus* is also of great interest for its ability to hydrolyze hydrocarbon and aromatic compounds under anaerobic conditions with petroleum as sole carbon source [22]. *M. hydrocarbonoclasticus* have been identified in microbial communities of MFCs fed with produced water (Barnett Shale), which gave a power of 47 mW/m² and COD removal efficiency of 68% [22]. Additionally, the presence of *Halanaerobium praevalens* is reasonable as this bacterium has already been identified as electrogenic in an extremely saline MFC [22,45]. *H. praevalens* is of interest because of its ability to reduce a variety of nitro-substituted aromatic compounds at a high rate, and to degrade organic pollutants [45]. The halophilic bacterium *Halomonas sp* found in B3 is also of great concern. In fact, Uma Maheswari et al. [46] reported for the first time that *Halomonas sp*, isolated from coastal areas in Tuticorin and capable of growing in 20% of salinity, possess particular electrochemical property in which salt is degraded by the microorganism, and the produced chemical energy was converted into electrical energy. Authors also demonstrated that at the same time salt water gets desalinated and the bacterium produce a maximum voltage up 1.42 V after five days.

4. Conclusion

We demonstrate in this study the enrichment of efficient exoelectrogenic bacteria from HSCE able to produce high current density (6.98 A/m²) under optimized conditions (salinity 165 g/L, temperature 45 °C and inoculum size 20%) by applying RSM. These statistical techniques are powerful in elucidating the interactive effects among the variables studied and thus improving the performance of BES.

The most abundant species in biofilm obtained under optimized conditions were *Psychrobacter aquaticus*, *Halanaerobium praevalens*, *Psychrobacter alimantarius*, and *Marinobacter hydrocarbonoclasticus*. As halothermotolerant bacteria, these strains could be suitable candidates for the design of halothermotolerant bioanodes and economically-efficient microbial electrochemical technologies for treatment and electricity generation from highly saline, high temperature wastewaters and for the development of microbial desalination cells (MDCs).

Acknowledgements

The authors gratefully thank the European commission, the French ANR [ANR-15-NMED-0010], and the Ministry of High Education and Scientific Research of the Tunisian Republic [grant number LR11ES31] for their financial support within the framework of the WE-MET project (ERANETMED 2015 European call 14-035).

Appendix A. Supplementary data

Supplementary data to this article can be found online at <https://doi.org/10.1016/j.bioelechem.2019.05.015>.

References

- [1] E. Roubaud, R. Lacroix, S. Da Silva, A. Bergel, R. Basséguy, B. Erable, Catalysis of the hydrogen evolution reaction by hydrogen carbonate to decrease the voltage of microbial electrolysis cell fed with domestic wastewater, *Electrochim. Acta* 275 (2018) 32–39, <https://doi.org/10.1016/j.electacta.2018.04.135>.
- [2] M. Grattieri, S.D. Minter, Microbial fuel cells in saline and hypersaline environments: advancements, challenges and future perspectives, *Bioelectrochemistry*. (2018) <https://doi.org/10.1016/j.bioelechem.2017.12.004>.
- [3] R. Rousseau, C. Santaella, A. Bonnafous, W. Achouak, J.J. Godon, M.L. Delia, A. Bergel, Halotolerant bioanodes: the applied potential modulates the electrochemical characteristics, the biofilm structure and the ratio of the two dominant genera, *Bioelectrochemistry*. 112 (2016) 24–32, <https://doi.org/10.1016/j.bioelechem.2016.06.006>.
- [4] A. Baudler, M. Langner, C. Rohr, A. Greiner, U. Schroder, Metal-polymer hybrid architectures as novel anode platform for microbial electrochemical technologies, *ChemSusChem*. (2016) 1–6, <https://doi.org/10.1002/cssc.201600814>.
- [5] O. Lefebvre, Z. Tan, S. Kharkwal, H.Y. Ng, Effect of increasing anodic NaCl concentration on microbial fuel cell performance, *Bioresour. Technol.* 112 (2012) 336–340, <https://doi.org/10.1016/j.biortech.2012.02.048>.
- [6] A. Vijay, S. Arora, S. Gupta, M. Chhabra, Halophilic starch degrading bacteria isolated from Sambhar Lake, India, as potential anode catalyst in microbial fuel cell: a promising process for saline water treatment, *Bioresour. Technol.* 256 (2018) 391–398, <https://doi.org/10.1016/j.biortech.2018.02.044>.
- [7] E. Blanchet, F. Duquenne, Y. Rafrali, L. Etcheverry, B. Erable, A. Bergel, Importance of the hydrogen route in up-scaling electrosynthesis for microbial CO₂ reduction, *Energy Environ. Sci.* 8 (2015) 3731–3744, <https://doi.org/10.1039/c5ee03088a>.
- [8] R. Rousseau, C. Santaella, W. Achouak, J.J. Godon, A. Bonnafous, A. Bergel, M.L. Délia, Correlation of the electrochemical kinetics of high-salinity-tolerant bioanodes with the structure and microbial composition of the biofilm, *ChemElectroChem*. 1 (2014) 1966–1975, <https://doi.org/10.1002/celec.201402153>.
- [9] S. Chen, G. He, Q. Liu, F. Harnisch, Y. Zhou, Y. Chen, M. Hanif, S. Wang, X. Peng, H. Hou, U. Schröder, Layered corrugated electrode macrostructures boost microbial bioelectrocatalysis, *Energy Environ. Sci.* 2 (2012) 9769–9772, <https://doi.org/10.1039/c2ee23344d>.
- [10] Y. Yuan, S. Zhou, Y. Liu, J. Tang, Nanostructured Macroporous Bioanode Based on Polyaniline- Modi fi ed Natural Loofah Sponge for High-Performance Microbial Fuel Cells, 2013.
- [11] S.F. Ketep, A. Bergel, A. Calmet, All, stainless steel foam increases the current produced by microbial bioanodes in bioelectrochemical systems, *Energy Environ. Sci.* 7 (2014) 1633, <https://doi.org/10.1039/c3ee44114h>.
- [12] S.A. Patil, F. Harnisch, B. Kapadnis, U. Schröder, Biosensors and bioelectronics electroactive mixed culture biofilms in microbial bioelectrochemical systems: the role of temperature for biofilm formation and performance, *Biosens. Bioelectron.* 26 (2010) 803–808, <https://doi.org/10.1016/j.bios.2010.06.019>.
- [13] A.M. Olliot, B. Erable, Increasing the temperature is a relevant strategy to form microbial anodes intended to work at room temperature, *Electrochim. Acta* (2017) <https://doi.org/10.1016/j.electacta.2017.10.110>.
- [14] H. Liu, S.A. Cheng, B.E. Logan, Power generation in fed-batch microbial fuel cells as a function of ionic strength, temperature, and reactor configuration, *Environ. Sci. Technol.* 39 (2005) 5488–5493, <https://doi.org/10.1021/es050316c>.
- [15] O. Adelaja, T. Keshavarz, G. Kyazze, The effect of salinity, redox mediators and temperature on anaerobic biodegradation of petroleum hydrocarbons in microbial fuel cells, *J. Hazard. Mater.* 283 (2015) 211–217, <https://doi.org/10.1016/j.jhazmat.2014.08.066>.
- [16] M. Olliot, S. Galier, H.R. De Balmann, A. Bergel, Ion transport in microbial fuel cells: key roles, theory and critical review, *Appl. Energy* 183 (2016) 1682–1704, <https://doi.org/10.1016/j.apenergy.2016.09.043>.
- [17] N.A. Shehab, J.F. Ortiz-madina, K. Katuri, A.R. Hari, B.E. Logan, P.E. Saikaly, Enrichment of extremophilic exoelectrogens in microbial electrolysis cells using Red Sea brine pools as inocula, *Bioresour. Technol.* (2017) <https://doi.org/10.1016/j.biortech.2017.04.122>.
- [18] H. Cherif, M. Neifar, H. Chouchane, et al., Extremophile diversity and biotechnological potential from desert environments and saline systems of southern Tunisia, in: V. Ravi, D. Durvasula, V. Subba Rao (Eds.), *Extremophiles: From Biology to Biotechnology*, CRC Publishers, Boca Raton, FL 2018, pp. 33–64, 2018.
- [19] K. Dai, J.L. Wen, F. Zhang, X.W. Ma, X.Y. Cui, Q. Zhang, T.J. Zhao, R.J. Zeng, Electricity production and microbial characterization of thermophilic microbial fuel cells, *Bioresour. Technol.* 243 (2017) 512–519, <https://doi.org/10.1016/j.biortech.2017.06.167>.
- [20] J.P. Badalamenti, R. Krajmalnik-brown, C.I. Torres, Generation of high current densities by pure cultures of anode-respiring Geobacter spp. Under alkaline and saline conditions, *MBio*. 4 (2013) 1–8, <https://doi.org/10.1128/mBio.00144-13>.Editor.
- [21] M. Pierra, Successful enrichment procedure for electroactive biofilm formation from environmental sample, *Chem. Eng. Commun.* 204 (1) (2015) <https://doi.org/10.1080/00986445.2016.1236336>.
- [22] O. Monzon, Y. Yang, J. Kim, A. Heldenbrand, Q. Li, P.J.J. Alvarez, Microbial fuel cell fed by Barnett Shale produced water: power production by hypersaline autochthonous bacteria and coupling to a desalination unit, *Biochem. Eng. J.* 117 (2017) 87–91, <https://doi.org/10.1016/j.bej.2016.09.013>.
- [23] M.A. Bezerra, R. Erthal, E. Padua, L. Silveira, L. Am, Talanta Response Surface Methodology (RSM) as a Tool for Optimization in Analytical Chemistry, vol. 76, 2008 965–977, <https://doi.org/10.1016/j.talanta.2008.05.019>.
- [24] E.J. Martínez-Conesa, V.M. Ortiz-Martínez, M.J. Salar-García, F.J. Hernández-Fernández, L.J. Lozano, G.A. Carlos, Box-Behnken Design-Based Model For Predicting Power Performance in Microbial Fuel Cells Using Wastewater, *Chemical*

- Engineering Communications, 2016 97–104, <https://doi.org/10.1080/00986445.2016.1236336>.
- [25] Y. Chen, P. Tsai, Y. Huang, P. Wu, Optimization and Validation of High- Performance Chromatographic Condition for Simultaneous Determination of Adapalene and Benzoyl Peroxide by Response Surface Methodology, 2015 1–9, <https://doi.org/10.1371/journal.pone.0120171>.
- [26] Y. Chen, P. Tsai, Y. Huang, P. Wu, Optimization and Validation of High- Performance Chromatographic Condition for Simultaneous Determination of Adapalene and Benzoyl Peroxide by Response Surface Methodology, 2015 1–9, <https://doi.org/10.1371/journal.pone.0120171>.
- [27] T. Yang, L. Sheng, Y. Wang, K.N. Wyckoff, C. He, Characteristics of cadmium sorption by heat-activated red mud in aqueous solution, *Sci. Rep.* (2018) 1–13, <https://doi.org/10.1038/s41598-018-31967-5>.
- [28] H. Chouchane, M. Mahjoubi, B. Ettoumi, M. Neifar, A. Cherif, A novel thermally stable heteropolysaccharide-based bioflocculant from hydrocarbonoclastic strain *Kocuria rosea* BU22S and its application in dye removal, *Environ. Technol.* 3330 (2017) 1–14, <https://doi.org/10.1080/09593330.2017.1313886>.
- [29] H. Chouchane, A. Najjari, M. Neifar, H. Cherif, R. Askri, F. Naili, H.I. Ouzari, A. Cherif, Unraveling the characteristics of a heteropolysaccharide-protein from an Haloarchaeal strain with flocculation effectiveness in heavy metals and dyes removal, *Environ. Technol.* (2018) 1–37, <https://doi.org/10.1080/09593330.2018.1556742>.
- [30] M. Ben Abdallah, F. Karray, N. Mhiri, N. Mei, M. Quéménéur, J.L. Cayol, G. Erauso, J.L. Tholozan, D. Alazard, S. Sayadi, Prokaryotic diversity in a Tunisian hypersaline lake, Chott El Jerid, *Extremophiles*. 20 (2016) 125–138, <https://doi.org/10.1007/s00792-015-0805-7>.
- [31] B. Erable, A. Bergel, Bioresource technology first air-tolerant effective stainless steel microbial anode obtained from a natural marine biofilm, *Bioresour. Technol.* 100 (2009) 3302–3307, <https://doi.org/10.1016/j.biortech.2009.02.025>.
- [32] B. Erable, M.A. Roncato, W. Achouak, A. Bergel, Sampling Natural Biofilms: A New Route to Build Efficient Microbial Anodes, 43, 2009 3194–3199.
- [33] S.L.C. Ferreira, R.E. Bruns, H.S. Ferreira, G.D. Matos, J.M. David, G.C. Brand, E.G.P. Silva, P.S. Reis, A.S. Souza, W.N.L. Santos, Box-Behnken design : An Alternative for the Optimization of Analytical Methods, 597, 2007 179–186, <https://doi.org/10.1016/j.jaca.2007.07.011>.
- [34] D. Mathieu, J. Nony, R. Phan-Tan-Luu, NEMROD-W Software, LPRAI, Marseille, 2000.
- [35] S.L.C. Ferreira, R.E. Bruns, H.S. Ferreira, G.D. Matos, J.M. David, G.C. Brand, E.G.P. Silva, P.S. Reis, A.S. Souza, W.N.L. Santos, Box-Behnken Design : An Alternative for the Optimization of Analytical Methods, 597, 2007 179–186, <https://doi.org/10.1016/j.jaca.2007.07.011>.
- [36] L.V. Candiot, M.M. De Zan, M.S. Cámara, C. Goicoechea, Talanta experimental design and multiple response optimization. Using the desirability function in analytical methods development, *Talanta*. 124 (2014) 123–138, <https://doi.org/10.1016/j.talanta.2014.01.034>.
- [37] G.I. Danmaliki, T.A. Saleh, A.A. Shamsuddeen, Response surface methodology optimization of adsorptive desulfurization on nickel / activated carbon, *Chem. Eng. J.* (2016) <https://doi.org/10.1016/j.cej.2016.10.141>.
- [38] R.H. Myers, D.C. Montgomery, *Response Surface Methodology: Process and Product Optimization Using Designed Experiments* (Wiley Series in Probability and Statistics), Wiley, New York, 2009.
- [39] B.E. Logan, *Essential Data and Techniques for Conducting Microbial Fuel Cell and Other Types of Bioelectrochemical System Experiments*, vol. 16802, 2012 988–994, <https://doi.org/10.1002/cssc.201100604>.
- [40] A. Larrosa, L.J. Lozano, K.P. Katuri, I. Head, K. Scott, C. Godinez, On the repeatability and reproducibility of experimental two-chambered microbial fuel cells, *Fuel*. 88 (2009) 1852–1857, <https://doi.org/10.1016/j.fuel.2009.04.026>.
- [41] J.F. Miceli, P. Parameswaran, D.W. Kang, R. Krajmalnik-Brown, C.I. Torres, Enrichment and analysis of anode-respiring bacteria from diverse anaerobic inocula, *Environ. Sci. Technol.* 46 (2012) 10349–10355, <https://doi.org/10.1021/es301902h>.
- [42] N. Shehab, D. Li, G.L. Amy, B.E. Logan, P.E. Saikaly, Characterization of bacterial and archaeal communities in air-cathode microbial fuel cells, open circuit and sealed-off reactors, *Appl. Microbiol. Biotechnol.* 97 (2013) 9885–9895, <https://doi.org/10.1007/s00253-013-5025-4>.
- [43] A.C. Martinez, E. Trably, N. Bernet, E. Trably, N. Bernet, High Current Density Via Direct Electron Transfer by the Halophilic Anode Respiring Bacterium *Geothalobacter Subterraneus* to Cite this Version, 2015.
- [44] A. Lasa, J.L. Romalde, Genome sequence of three *Psychrobacter* sp. strains with potential applications in bioremediation, *Genomics Data*. 12 (2017) 7–10, <https://doi.org/10.1016/j.gdata.2017.01.005>.
- [45] J.G. Zeikus, P.W. Hegge, T.E. Thompson, T.J. Phelps, T.A. Langworthy, Isolation and description of *Haloanaerobium praevalens* gen. Nov. and sp. nov., an obligately anaerobic halophile common to Great Salt Lake sediments, *Curr. Microbiol.* 9 (1983) 225–233, <https://doi.org/10.1007/BF01567586>.
- [46] R.U. Maheswari, C. Mohanapriya, P. Vijay, K.S. Rajmohan, M. Gopinath, R.U. Maheswari, C. Mohanapriya, P. Vijay, K.S. Rajmohan, M. Gopinath, Bioelectricity Production and Desalination of *Halomonas* sp. – the Preliminary Integrity Approach, 7269, 2016 <https://doi.org/10.1080/17597269.2016.1242687>.